JOURNAL OF SOLID STATE CHEMISTRY 63, 8–15 (1986)

Structural and Dynamical Studies of δ-Bi_2O_3 Oxide Ion Conductors

I. The Structure of $(Bi_2O_3)_{1-x}(Y_2O_3)_x$ as a Function of x and Temperature

P. D. BATTLE,*,[1] C. R. A. CATLOW,† J. W. HEAP,‡ AND L. M. MORONEY†

**Department of Inorganic and Structural Chemistry, Leeds University, Leeds LS2 9JT, United Kingdom; †Department of Chemistry, University College London, 20 Gordon Street, London WC1H 0AJ, United Kingdom; and ‡Inorganic Chemistry Laboratory, Oxford University, South Parks Road, Oxford, OX1 3QR, United Kingdom*

Received June 5, 1985; in revised form September 10, 1985

We report the results of both Bragg and diffuse neutron scattering studies of the superionic solid solution, $(Bi_2O_3)_{1-x}(Y_2O_3)_x$. The Bragg data for polycrystalline samples show that the structural features observed previously in $(Bi_2O_3)_{0.73}(Y_2O_3)_{0.27}$ are present across the entire range of the solid solution, $0.25 < x < 0.42$. The number of ⟨111⟩-displaced anions in the defect fluorite structure decreases with increasing Y^{3+} content whereas the extent of short-range ordering on the anion sublattice increases. Both of these observations are consistent with the decrease in oxide ion conductivity which occurs as x increases. The basic crystal structure does not change between room temperature and 1023 K, although the unit cell volume increases by 3.78% for $x = 0.27$, and the number of ⟨111⟩-displaced anions increases, again consistent with the enhanced conductivity observed at high temperatures. It is suggested that Y^{3+} stabilizes the fluorite structure by ordering the vacancies on the oxygen sublattice in chains along the ⟨111⟩ and ⟨110⟩ directions.

Introduction

The high-temperature δ phase of Bi_2O_3 (stable above 1003 K) is the best oxide ion conductor known (*1*), with a conductivity of $\sim 1\ \Omega^{-1}\ cm^{-1}$ at 1023 K compared to a value of $\sim 10^{-4}\ \Omega^{-1}\ cm^{-1}$ for the widely used CaO/ZrO_2 system (*2*). Our previous neutron diffraction study (*3*) showed that δ-Bi_2O_3 has a defective fluorite structure in which 43% of the regular anion sites are randomly occupied, the remaining 1.28 oxide ions per unit cell being displaced from their ideal positions along ⟨111⟩ directions. This high level of disorder is clearly related to the exceptional oxide ion conductivity.

A number of cation dopants lower the temperature of transition from the poorly conducting low-temperature phase to the superionic, δ phase (*1*). For example, Y_2O_3-doped Bi_2O_3 is stable with the face-centered-cubic fluorite-like structure at room temperature for dopant levels of between 25 and 42 mole%. However, the presence of the dopant ions raises the Arrhenius energy for oxygen migration and hence lowers the ionic conductivity. Our earlier work on $(Bi_2O_3)_{0.73}(Y_2O_3)_{0.27}$ (*3*) showed that the

[1] To whom correspondence should be addressed.

0022-4596/86 $3.00

number of ⟨111⟩-relaxed anions decreases when yttrium is introduced into the structure. There was also some evidence for cation relaxation along the ⟨100⟩ directions and for a small number of interstitial anions on 48i ($\frac{1}{2}$,v,v) sites. We have now extended our study to monitor the effects of dopant concentration and temperature on the structural properties of $(Bi_2O_3)_{1-x}(Y_2O_3)_x$. These effects have been investigated using both the Bragg scattering and diffuse neutron scattering techniques. The former gives information on the structure within the average unit cell whereas the diffuse neutron scattering reflects local departures from the average structure, that is short-range ordering of vacancies or cations.

Experimental

Polycrystalline samples of $(Bi_2O_3)_{1-x}(Y_2O_3)_x$ (x = 0.27, 0.34, 0.40) were prepared by firing the appropriate amounts of Bi_2O_3 and Y_2O_3 (Johnson Matthey "Specpure" reagents) in a platinum crucible at 1073 K for 5 hr, and then at 1143 K for 24 hr. The product was ground and fired at 1143 K for a further 24 hr before being annealed at 773 K for 1 day. The X-ray diffraction pattern of the final product showed only the lines characteristic of a face-centered cubic, fluorite-like structure. Analytical electron microscopy was used to confirm the homogeneity of the samples.

Neutron diffraction data were collected at room temperature (34 and 40% Y_2O_3) and 1023 K (27% Y_2O_3) using the constant wavelength (1.388 Å) diffractometer, D1A, at ILL, Grenoble. The experiments were repeated at the General Purpose Powder Diffractometer (GPPD) time-of-flight instrument at IPNS, Argonne, to obtain additional high Q data, as discussed in the next section. For the high-temperature experiments a sintered, rod-shaped sample was mounted in an air-filled quartz holder, similar to that described by Harwig (*4*) thus precluding reduction of the sample in the furnace. Gold foil was used to separate the sample and the quartz to prevent their reacting.

The diffuse scattering from the samples, $x = 0$ (1023 K), $x = 0.27$ (room temperature and 1023 K), and $x = 0.40$ (room temperature only) was recorded over the range $0.14 < Q < 2.56$ Å^{-1} using the instrument D7 at the ILL, operating at a wavelength of 4.75 Å. Data were also collected on a vanadium rod, cadmium foil, and an empty cylindrical aluminium container for use in normalizing the room-temperature results. Also, the diffuse scattering attributable to the empty quartz container and the furnace was measured for the high-temperature normalization.

An examination of the doped samples by electron diffraction failed to provide any evidence for superlattice formation thus suggesting that any ordering in the samples is over distances less than approximately 30 Å. It should be noted, however, that the electron scattering power of the oxygen sublattice is weak and it is not inconceivable that electron diffraction might fail to pick up long-range ordering on the oxygen sublattice.

Results

Bragg Scattering

These materials are highly disordered and yield relatively few Bragg reflections. The time-of-flight method permits the collection of data over a wider Q range than the constant wavelength method and thus offers distinct advantages for analysis of this system. Any additional data should reduce termination errors in the subsequent difference Fourier calculations and reduce the standard deviations on the occupation numbers and temperature factors obtained from the least-squares analysis of the data. However, time-of-flight data is character-

ized by non-Gaussian Bragg peaks superimposed upon a background function which increases exponentially with Q, and, thus, analysis of the data requires a more complex treatment of both peak shape and background than is necessary in the case of the constant wavelength data. These problems were exacerbated in this work by the additional, strong modulation of the background by diffuse scattering from the samples and, in the high-temperature experiment, from the quartz sample holder. This precluded our fitting the background with the usual analytical functions (*5*) and, instead, an estimate was made of the background on either side of the Bragg peaks with the intervening points being obtained by interpolation. In spite of this difficulty, we were able to refine the structures of the solid solutions using both the time-of-flight and the constant wavelength data sets. In the case of the room-temperature experiments, the time-of-flight results were in excellent agreement with those obtained for the D1A data. In the case of the experiment at 1023 K, the counting statistics associated with the time-of-flight data were better than those from D1A and the least-squares refinements were consequently more stable. Much of this improvement in statistics can be ascribed to the different instrument geometries in that the incident and scattered beams do not have to pass through the furnace casing on GPPD whereas they do on D1A. Thus, the results presented below for the high-temperature study were obtained by analysis of the GPPD data.

The diffraction patterns observed on D1A at room temperature from both 40 and 34% Y_2O_3-doped Bi_2O_3 consisted of 19 well resolved Bragg peaks (22 reflections) and profile analysis (*7*) was therefore used only to refine the value of the unit cell parameter, a_0. The structural parameters were refined using the least-squares-fitting program developed by Wiseman (*6*) which uses the integrated intensity under each peak. For each composition, we made the initial assumption that the structure is fluorite-based with a random 25% of the anion sites vacant and a statistical distribution of bismuth and yttrium over the cation sites. In all the refinements, the stoichiometry of the samples was constrained to be $(Bi/Y)_2O_3$. Difference Fourier maps calculated after refinement of the scale factor and isotropic temperature factors in space group $Fm3m$ showed that these two solid solutions were structurally very similar to the 27% Y-doped sample studied previously and we consequently introduced the following three features into our model: the presence of displaced anions on $32f$ (xxx) sites; a displacement of the cations to $24e$ ($x00$) sites; and a small number of interstitial atoms on $48i$ ($\frac{1}{2}xx$) sites. Least-squares refinements of occupation numbers, temperature factors and positional parameters gave R values of 1.6 and 1.9% for the 40 and 34% Y-doped samples, respectively. The final atomic coordinates, temperature factors, occupation numbers, and cell parameters are presented in Table I which, for completeness, includes the parameters determined previously for the 27% Y-doped sample and for δ-Bi_2O_3.

As is clearly illustrated in Fig. 1, the dis-

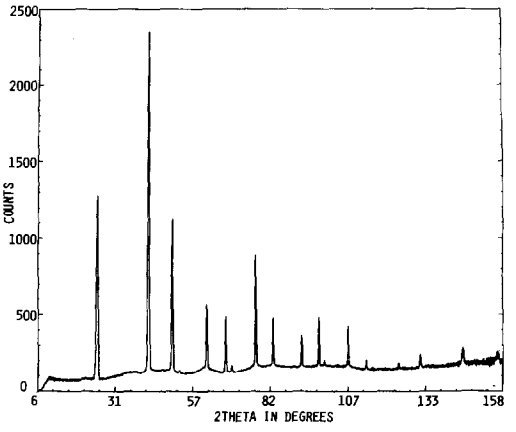

FIG. 1. D1A room temperature diffraction pattern of 40% Y_2O_3-doped Bi_2O_3.

TABLE I

STRUCTURAL PARAMETERS FOR $(Bi_2O_3)_{1-x}(Y_2O_3)_x$ AS A FUNCTION OF CONCENTRATION AND TEMPERATURE

	Pure Bi_2O_3	27% Y_2O_3	27% Y_2O_3	34% Y_2O_3	40% Y_2O_3
Temperature (K)	1023	1023	298	298	298
Lattice parameter a (Å)	5.6485(6)	5.5466(2)	5.4784(2)	5.4650(1)	5.4469(1)
Cation (24e,x,0,0)					
x	0.0	0.065(1)	0.048(4)	0.042(5)	0.046(3)
B (Å)	7.3(1)	0.3(2)	1.7(3)	2.1(4)	1.7(3)
Oxygen (8c,¼,¼,¼)					
B (Å)	11.8(7)	5.3(1)	5.3(2)	4.6(2)	4.6(2)
Occ.No.	1.72(9)	1.84(2)	2.01(6)	2.06(7)	2.33(6)
Oxygen (32f,x,x,x)					
x	0.354(3)	0.321(1)	0.319(3)	0.314(4)	0.320(4)
B (Å)	9.9(9)	4.8(4)	5.3(2)	4.6(2)	4.6(2)
Occ.No.	1.28(9)	1.00(2)	0.83(6)	0.73(8)	0.55(6)
Oxygen (48i,½,v,v)					
v	—	0.390(8)	0.316(10)	0.316(14)	0.288(23)
B (Å)	—	4.8(4)	5.3(2)	4.6(2)	4.6(2)
Occ.No.	—	0.16(2)	0.16(6)	0.20(11)	0.12(8)
R_I%	2.2	5.0	1.7	1.9	1.6

ordered nature of these materials leads to a rapid decrease in the Bragg scattering with increasing Q. This effect is even more pronounced at high temperatures: only 14 Bragg peaks (16 reflections) in the scattering from 27% Y-doped Bi_2O_3 were detected on the GPPD counter at $2\theta = 90°$. This is reflected in the large Debye-Waller factors obtained. Profile analysis of this high-temperature data gave a final weighted profile R factor of 7.5%. The lack of data necessitated a somewhat incomplete treatment of the thermal motion in the structure at high temperature; the cations were assumed to move in a harmonic potential and the B factors of the all displaced oxide ions were assumed to be the same although they were not constrained to have the same value as the regular lattice anions. The final parameters are presented in Table I.

Diffuse Scattering

The D7 diffuse scattering data were corrected for background scattering, counter efficiencies, angular dependent absorption, and volume density of scatterers and scaled to the vanadium incoherent cross section in the usual way (*8, 9*). Contributions to the total diffuse scattering from multiple scattering were calculated using the method of Blech and Averbach (*8*) and were found to be negligible (<1% of the total scattering). The incoherent scattering calculated from the individual σ(inc) is also small with $\sigma(0) = 0.0$, $\sigma(Bi) = 0.0072$, and $\sigma(Y) = 0.15$ barns. We assumed σ(inc) to be isotropic. However, the wavelength used in the D7 experiment (4.75 Å) did not exceed the Bragg cutoff with the result that the (111) and (200) reflections are detected at $2\theta = 98°$ and 121°, respectively. Using the method of de Novion (*10*), we calculated the double Bragg scattering profile over the measured Q range. This yields a smoothly varying function with no structure. Thus, although this shows that double Bragg scattering is not responsible for any of the peaks in the observed spectra, it does intro-

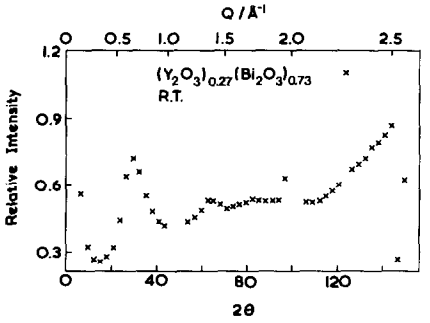

FIG. 2. Diffuse scattering for 27% Y_2O_3-doped Bi_2O_3 at room temperature.

duce difficulties in placing the differential scattering cross section onto an absolute scale. For this reason, only relative intensities are given.

Figures 2 and 3 show the resulting relative intensity versus Q plots for 27 and 40% Y_2O_3-doped Bi_2O_3, respectively. Both are characterized by a pronounced peak at $2\theta = 29°$ ($Q = 0.66$ Å^{-1}) which increases with increase in Y_2O_3 concentration. The smaller peak at $2\theta = 82°$ ($Q = 1.74$ Å^{-1}) also increases markedly with Y^{3+} content; the peak at $2\theta = 65°$ ($Q = 1.42$ Å^{-1}) appears to remain approximately constant in intensity.

The similarity of the scattering lengths of Bi^{3+} and Y^{3+} (0.86 and 0.80 $\times$ 10^{-12} cm, respectively) ensures that any diffuse scattering resulting from cation ordering will be weak and we thus attribute the observed structure in the D7 data to vacancy ordering on the oxygen sublattice. The peaks at $Q = 0.66$ and 1.74 Å^{-1}, which increase in intensity with Y^{3+} concentration, correspond to the $(\frac{1}{3},\frac{1}{3},\frac{1}{3})$ and (1,1,0) points in the reciprocal lattice. From the width at half maximum height of the $(\frac{1}{3},\frac{1}{3},\frac{1}{3})$ peak, we estimate the extent of the ordering in real space to be about 15–20 Å, i.e., about three lattice spacings. Calculations of the predicted diffuse scattering for simple models of vacancies distributed along the body diagonal, or face diagonal, or combinations of each, on the anion sublattice gave peaks at the correct Q values but never with the observed sharpness. This is not surprising in that the width of the peaks indicates that the observed ordering extends over 20 to 30 shells of anion neighbours and thus a large number of parameters may be required to describe ordering on this scale. Indeed, the sharpness of the peaks suggests that superlattice formation does occur (although undetected in the electron microscope) and that the intensity at $(\frac{1}{3},\frac{1}{3},\frac{1}{3})$ and (1,1,0) should be treated as Bragg scattering rather than diffuse scattering.

In Figs. 4 and 5 are shown the diffuse scattering obtained at 1043 K for pure Bi_2O_3 and 27% Y_2O_3-doped Bi_2O_3. The statistics for this data are worse than the room-temperature data partly because the diffuse scattering attributable to the sample was su-

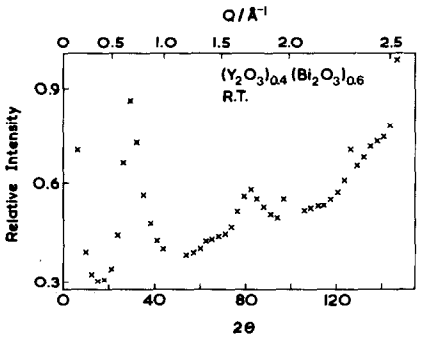

FIG. 3. Diffuse scattering for 40% Y_2O_3-doped Bi_2O_3 at room temperature.

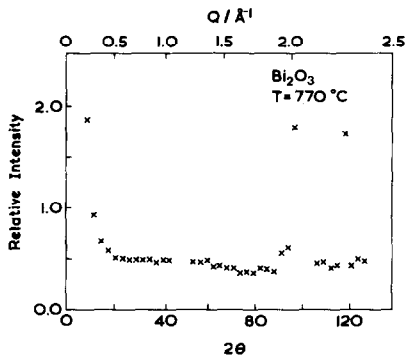

FIG. 4. Diffuse scattering for pure Bi_2O_3 at 1043 K.

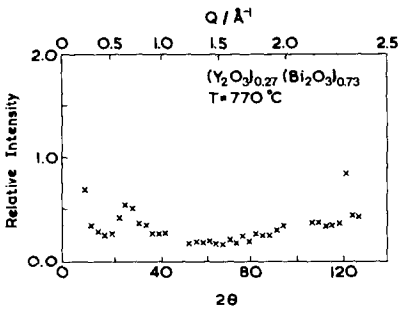

FIG. 5. Diffuse scattering for 27% Y_2O_3-doped Bi_2O_3 at 1043 K.

perimposed upon an intense diffuse background due to the quartz container which was subsequently subtracted. The δ-Bi_2O_3 data recorded at 1043 K shows no significant modulation of the diffuse scattering—the only structure in the spectra being that of the (111) and (200) Bragg peaks. However, there is evidence to suggest that short range ordering, possibly characteristic of α-Bi_2O_3, does persist at temperatures closer to the $\alpha \rightarrow \delta$ transition temperature of 730 K (*11, 12*). At 1023 K the 27% Y_2O_3-doped Bi_2O_3 sample has apparently lost some of the order observed at room temperature at $Q = 1.42$ Å^{-1} and $Q = 1.74$ Å^{-1} but the peak at $Q = 0.66$ Å^{-1} remains clearly evident.

Discussion

The Bragg Data

Although the standard deviations on the refined parameters presented in Table I are rather large, there is evidence to suggest that the number of ⟨111⟩-displaced oxide ions decreases with increasing yttrium concentration in the solid solution, as does the oxide ion conductivity. The concentration of ⟨110⟩-displaced interstitial anions is low and the variation across the composition range is within experimental error. The increased number of ⟨111⟩-displaced oxide ions is thus accompanied by a decrease in the fraction of the regular anion sites which are occupied, suggesting a conductivity mechanism based on the movement of anions between regular sites which is facilitated by the displacement of some ions off regular sites. The ⟨110⟩ anion displacements and ⟨100⟩ cation displacements can be related to the addition of Y_2O_3 to the phase; no ⟨110⟩ displacements were detected in the δ-Bi_2O_3 diffraction data.

The limited data available at 1023 K necessitate a cautious approach to the interpretation of the high-temperature results. It appears that the basic structure is unchanged between room temperature and 1023 K but there is evidence to suggest that the number of ⟨111⟩-relaxed anions is greater at the higher temperature as, of course, is the anion conductivity. This observation lends further support to the idea that the relaxation of oxide ions along ⟨111⟩ plays a crucial role in facilitating the transport process. The apparent increase in cation displacement and the decrease in the temperature factor of the metal are probably not significant, but rather artifacts of the refinement procedure, the level of correlation between the two parameters being 96%.

The unit cell constant is another structural parameter which correlates well with the observed conductivity, decreasing with increasing yttrium content. In the case of 27% Y-doped Bi_2O_3, the unit-cell parameter increases from 5.4784 to 5.5466 Å, a remarkably large fractional increase of 1.24%, between room temperature and 1023 K. This increase in unit cell volume will lower the Madelung potential of the lattice ions which will facilitate ion transport. The increase also indicates an exceptionally high anharmonicity in the interatomic force field which must be of significance in the interpretation of the ionic conductivity.

Diffuse Scattering

It is clear that the dopant material plays an important role in stabilizing the fluorite

structure, and we believe that our D7 data contain some important clues as to how this is achieved. It is instructive to consider first the C-type rare earth structure of Y_2O_3 itself. Although all of the Y^{3+} ions are coordinated to oxide ions at six corners of a cube, there are, in fact, two distinct cation environments in this structure. Specifically, for 25% of the Y^{3+} ions, the two vacant cube corners are separated by a body diagonal of the cube, whereas for the remaining 75% of the Y^{3+} ions, the two vacant sites lie along a face diagonal of the cube. The very existence of these anion cubes is reminiscent of the fluorite structure and it is not unreasonable to propose that small microdomains containing Y_2O_3-like anion ordering develop as the concentration of Y^{3+} in the host δ-Bi_2O_3 fluorite phase increases. The increase in intensity of the $(\frac{1}{3},\frac{1}{3},\frac{1}{3})$ reflection with the concentration of dopant is suggestive of increasing anion ordering along the ⟨111⟩ direction and the increasing intensity of the (110) reflection is consistent with anion ordering along the ⟨110⟩ direction (the face diagonal of the anion cube). Both types of ordering are clearly absent from pure δ-Bi_2O_3, where the D7 data are featureless at low Q values.

Unfortunately, the data we present in this paper are insufficient to characterize the structure in the microdomains fully. However, it is interesting to note that the three maxima in the diffuse scattering data can be indexed on a hexagonal unit cell with $a \sim 4.0$ Å and $c \sim 28.5$ Å, i.e. a unit cell with dimensions comparable to those of Bi_2O_3/Sm_2O_3 solid solutions (*13*). Unfortunately, the detailed structure of the anion sublattice in this material has still to be determined, but it appears that the structure of the microdomains in $(Bi_2O_3)_{1-x}(Y_2O_3)_x$ fluorite solid solutions may be related to the low-temperature rhombohedral structure of $(Bi_2O_3)_{1-x}(Sm_2O_3)_x$ solid solutions. We plan to investigate this in future EXAFS experiments. For the present, we can speculate

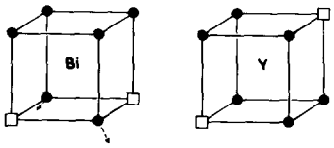

FIG. 6. Postulated distribution of vacancies in the Bi^{3+} and Y^{3+} coordination shells.

on the likely local ordering around the two different species of cation. The principal electronic difference between Y^{3+} and Bi^{3+} is that the former has a closed-shell electron configuration whereas the latter has a "lone pair" of electrons. In consequence, Y^{3+} prefers a regular coordination environment whereas the polarizable Bi^{3+} is often found in irregular environments with the lone pair directed toward a vacant coordination site. In the fluorite-related structure of δ-Bi_2O_3, it is reasonable to hypothesize that the lone pair can be more readily accommodated when the Bi^{3+} ion is surrounded by six oxide ions and two face-diagonal vacancies rather than six-oxide ions and two body-diagonal vacancies; that is the arrangement in Fig. 6a is preferred. It is not easy to visualize the lone pair in a coordination site in the centrosymmetric case where the two vacancies lie along the body-diagonal of the anion cube (Fig. 6b). It is reasonable to suggest that the two anions which share a cube face with the two vacancies in Fig. 6a will relax slightly along ⟨111⟩ directions, as observed in the analysis of our Bragg data. To summarize, we envisage pure δ-Bi_2O_3 to have an anion sublattice with only limited vacancy pair ordering which we did not detect in our high-temperature D7 experiment; however, we did observe the resultant ⟨111⟩ anion displacements in our Bragg scattering experiments. As Y_2O_3 dopant is introduced, anion ordering occurs along both ⟨111⟩ and ⟨110⟩ directions and over distances large enough to give rise to what is effectively Bragg scattering. The Y^{3+} cations may be associated with either ⟨111⟩ or ⟨110⟩ vacancy strings,

as in pure Y_2O_3, but we tentatively suggest that the Bi^{3+} ions are more likely to be associated with ⟨110⟩ strings in order to accommodate the stereochemically active lone pair of electrons. The concentration of ⟨111⟩-displaced anions increases with increasing bismuth concentration, as required by the model described here, and there is a concomitant drop in the oxide ion conductivity as the number of occupied regular anion sites increases.

Acknowledgments

We would like to thank Dr. John Kilner and Dr. John Faber, Jr., for useful discussions. Dr. Alan Hewat, Dr. Jerry Skarnulis, and Herr Prof. Dr. O. Schaerpf provided experimental assistance and the SERC provided financial assistance with Grants GR/D/02041 and GR/C/48585.

References

1. T. Takahashi and H. Iwahara, *Mat. Res. Bull.* **13,** 1447 (1978).
2. J. A. Kilner and B. C. H. Steele, "Non Stoichiometric Oxides" (O. T. Sorensen, Ed.), Chap. 3, Academic Press, New York, 1981.
3. P. D. Battle, C. R. A. Catlow, J. Drennan, and A. D. Murray, *J. Phys. C* **16,** L561 (1983).
4. H. A. Harwig, *Z. Anorg. Allg. Chem.* **444,** 151 (1978).
5. R. B. Von Dreele, J. D. Jorgensen, and C. G. Windsor, *J. Appl. Crystallogr.* **15,** 581 (1982).
6. P. J. Wiseman, D. Phil. Thesis. Oxford University, 1974.
7. H. M. Rietveld, *J. Appl. Crystallogr.* **2,** 65 (1969).
8. I. A. Blech and B. L. Averbach, *Phys. Rev. A* **137,** A1113 (1965).
9. B. E. F. Fender, "Chemical Applications of Thermal Neutron Scattering" (B. T. M. Willis, Ed.), Chap. 11, Oxford Univ. Press, London, 1973.
10. C-H. de Novion, personal communication.
11. C. R. A. Catlow and J. Drennan, ILL Annual Report. 7-07-48, Grenoble, France, 1982.
12. M. Tsubaki and K. Koto, *Mat. Res. Bull.* **19,** 1613 (1984).
13. H. Iwahara, T. Esaka, T. Sato, and T. Takahashi, *J. Solid State Chem.* **39,** 173 (1981).